Danmarks Tekniske Universitet

DTU

Assignment 4

Authors

Bao Ngoc Thai - s242504
Erika Samantha Young - s242666
Alex Michel Louis Pardon - s243245

July 14, 2025

Contents

1 Parameter estimation in state-space model **1**
1.1 Simulate 5 independent realizations of the process 1
1.2 Simulate a single realization of the process described 1
1.3 Estimate parameters by maximizing the (log-)likelihood of the observations 2
1.4 Estimate parameters from noisy observations 3
1.5 Simulate with system noise from a student's t-distribution 5

2 Parameter estimation in state-space model **6**
2.1 Exploratory analysis of the data 6
2.2 Estimate a 1-D state-space model 7
2.3 Expand to a 2-dimensional state-space model 9
2.4 Interpret the two reconstructed states 10

1 Parameter estimation in state-space model

In this part of the assignment, the input (u_{t-1}) is assumed as constant and absorbed into a bias term, resulting in a scalar system of the form below:

$$X_t = aX_{t-1} + b + e_{1,t}$$

where:

- a is the scalar state transition coefficient,
- b is a scalar bias term
- $e_{1,t} \sim \mathcal{N}(0, \sigma_1^2)$ is standard Gaussian noise

The observation model used in this part follows the form below:

$$Y_t = X_t + e_{2,t}$$

1.1 Simulate 5 independent realizations of the process

Figure 1 shows the 5 simulations of up to n = 100 time steps, using the parameter values a = 0.9, b = 1, $\sigma_1 = 1$, and an initial value $X_0 = 5$.

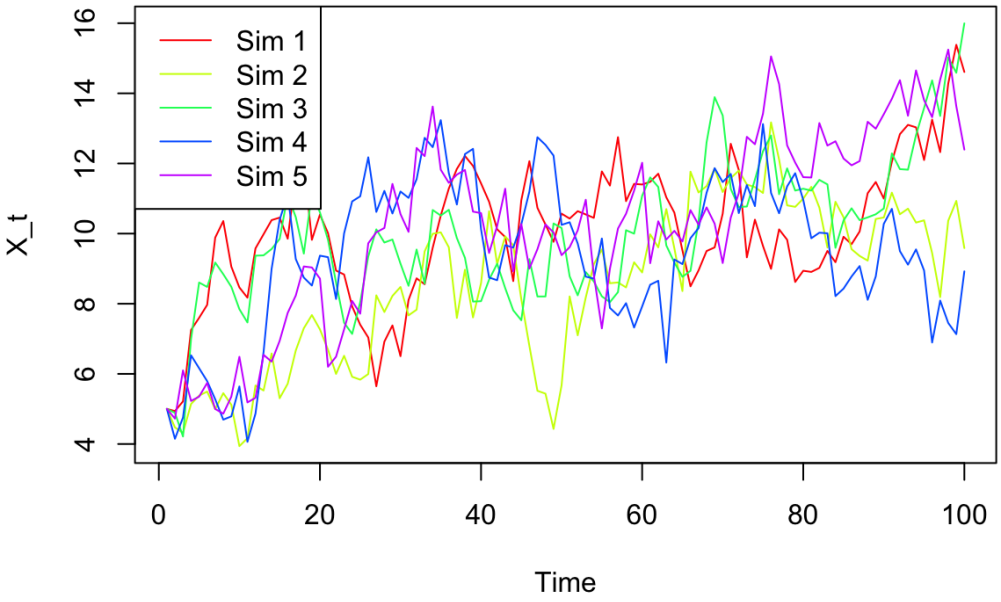

Figure 1: Five simulations of above process with a = 0.9, b = 1, $\sigma_1 = 1$, and an initial value $X_0 = 5$.

1.2 Simulate a single realization of the process described

Figure 2 shows latent state and noisy observations of up to n = 100 time steps, using the parameter values a = 0.9, b = 1, $\sigma_1 = \sigma_2 = 1$, and an initial value $X_0 = 5$. The plot shows both the latent state X_t (red, dashed line) and the observations Yt (blue, solid line) over time. The observations appear noisy and fluctuate more than the true state. The true state appears relatively smooth, due to the lack of noise layer. Despite the noise, the general trend loosely follows, indicating that observations carry meaningful information about the latent process. The difference between the latent states and the observations at any time point represents the observation noise. Figure 3 presenting the ACF and PACF of the residuals shows that the residuals are most likely white noise, confirming the assumptions of the state-space model.

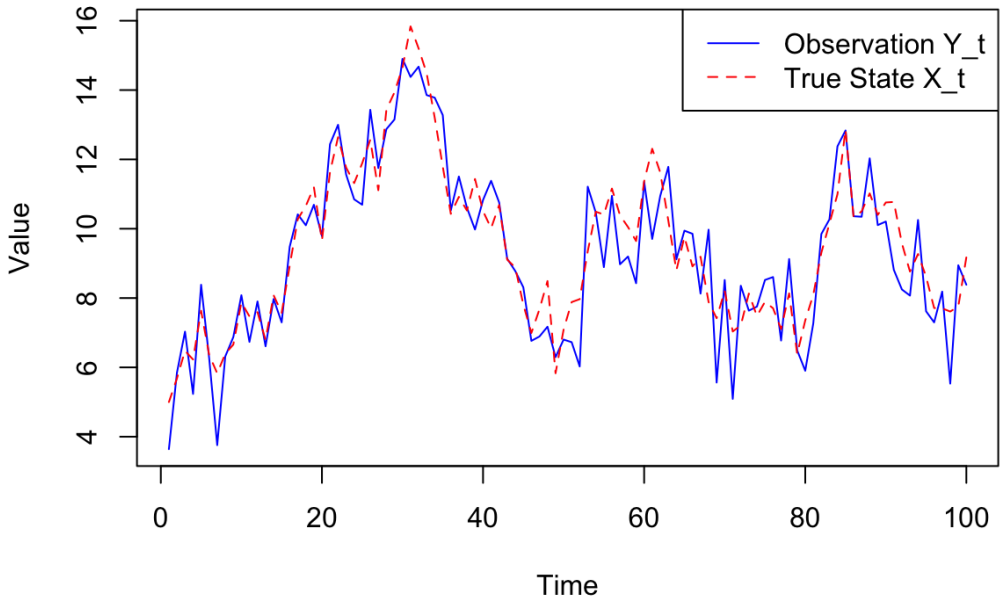

Figure 2: Latent state and observations with a = 0.9, b = 1, $\sigma_1 = \sigma_2 = 1$, and an initial value $X_0 = 5$.

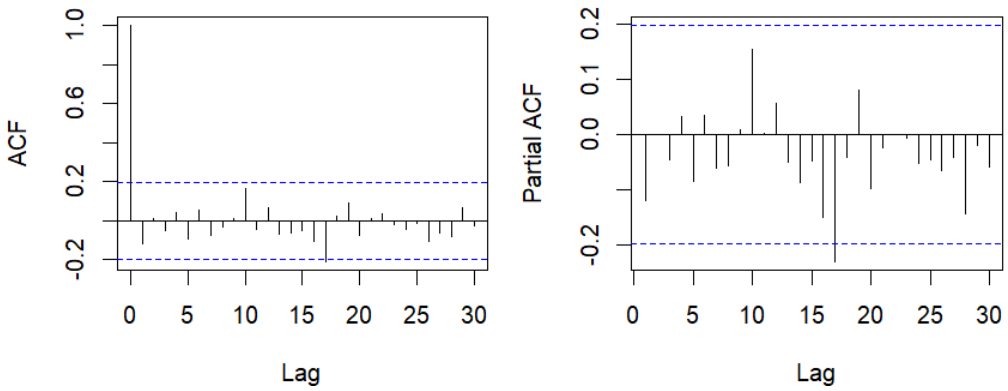

Figure 3: Residuals between latent states and observations: white noise.

1.3 Estimate parameters by maximizing the (log-)likelihood of the observations

Figure 4 shows the predictions of the latent state X_t using Kalman filter based on noisy observations Y_t, along with 95% confidence intervals. The red line represents the one-step-ahead predicted state $\hat{X}_{t|t-1}$, and the shaded pink area denotes the associated uncertainty region (i.e., $\pm 1.96 \cdot \sqrt{P_{t|t-1}}$). The true latent state X_t is shown as a dashed black line, and the noisy observations Y_t are shown in blue.

The Kalman filter operates recursively in two steps: a prediction step, where it projects the state forward using the system model, and an update step, where it adjusts the prediction based on the new observation and the associated uncertainties. This allows the Kalman filter to combine prior knowledge with incoming data, producing an estimate of the hidden state and a corresponding measure of uncertainty.

It can be observed in Figure 4 that the confidence interval appropriately widens or tightens depending on the uncertainty in the state estimate, reflecting how the filter balances model prediction and observation noise. In periods with more observation variability or faster dynamics, the CI becomes wider, reflecting greater uncertainty. However, the true state remains mostly within the 95% CI, indicating that the filter is generally well-calibrated and effectively reconstructs the latent state from noisy data.

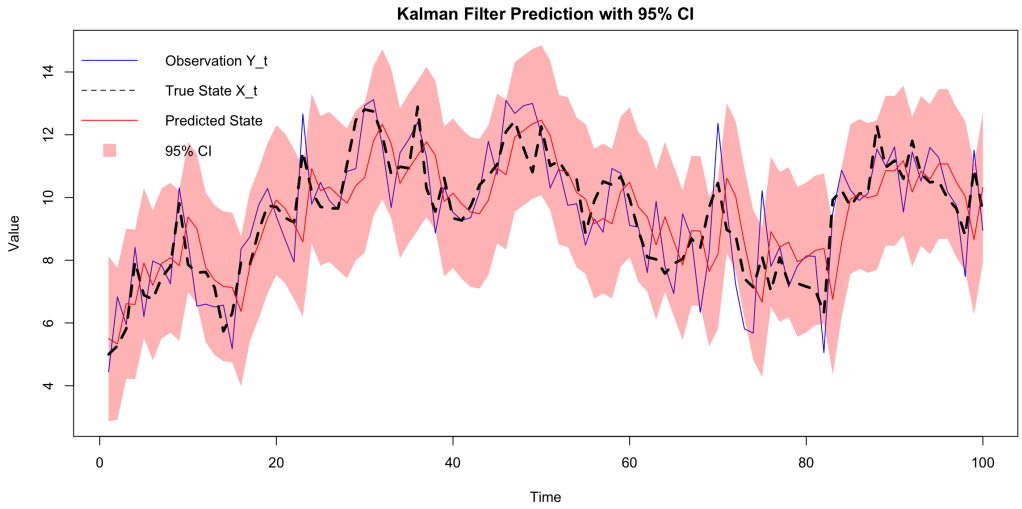

Figure 4: Kalman Filter prediction (with 95% CI) observations and true state.

1.4 Estimate parameters from noisy observations

The negative log-likelihood for a 1-D linear Gaussian state space model is:

$$\mathcal{L} = -\frac{1}{2}\sum_{t=1}^{T}\left[\log S_t + \frac{(y_t - \hat{y}_t)^2}{S_t} + \log(2\pi)\right]$$

Parameters a, b, and σ_1 of the state equation were estimated using this maximum likelihood. A total of 100 datasets were simulated from the known parameter values and the Kalman filter was used to compute the likelihood for each realization. The `optim()` function was applied to maximize the likelihood with respect to the model parameters. Known parameter combinations of (1) $a = 1, b = 0.9, \sigma_1 = 1$, (2) $a = 5, b = 0.9, \sigma_1 = 1$, and (3) $a = 1, b = 0.9, \sigma_1 = 5$ were simulated.

The boxplots in Figure 5 show the distribution of the three parameter combination estimates across simulations. Note that the y-axis scale differs between plots. The red, green, and blue dashed lines indicate the true parameter values of a, b, and σ_1, respectively. The line for a and σ_1 are overlapping in the first plot, as both values are 1.

Under the baseline setting ($a = 1, b = 0.9, \sigma_1 = 1$), the estimates closely align with the true parameter values. The distribution of estimates is centered and reasonably tight, with minimal bias. This confirms that the Kalman filter provides accurate and consistent estimates when the underlying assumptions are satisfied. However, when the autoregressive coefficient is increased to $a = 5$, the estimation procedure fails. This suggests that the Kalman filter, which assumes a stable process, is not well-suited to handle explosive dynamics or systems operating far from stationarity. In the high noise case ($\sigma_1 = 5$), the filter still manages to estimate a well, but the estimates for b and σ_1 exhibit large variability and bias. This reflects the difficulty in separating deterministic trends from high process noise in short time series. Overall, the Kalman filter performs well under moderate noise and stable dynamics, but its reliability deteriorates when these assumptions are violated.

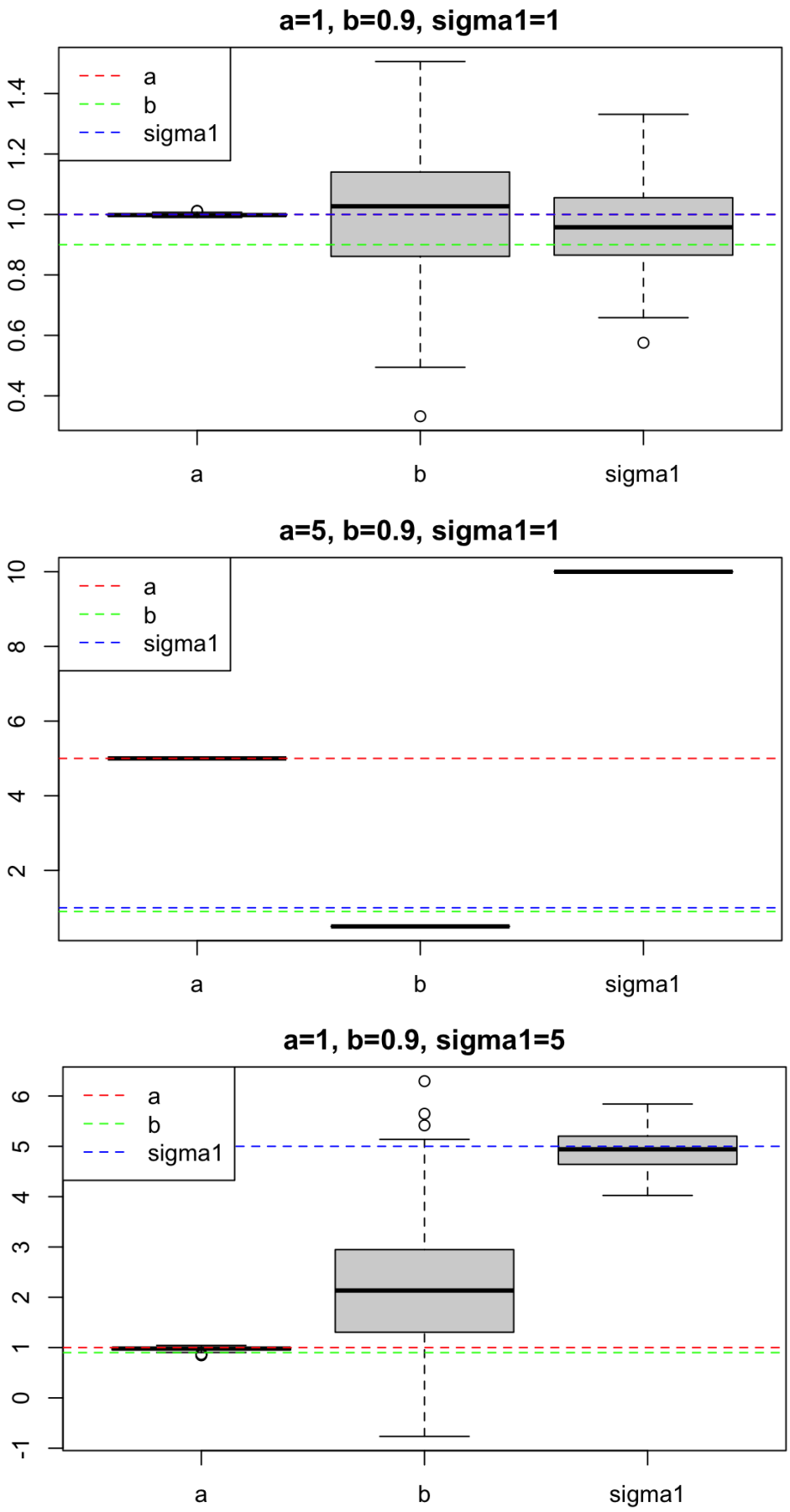

Figure 5: Parameter Estimates for Different Known Parameter Values

1.5 Simulate with system noise from a student's t-distribution

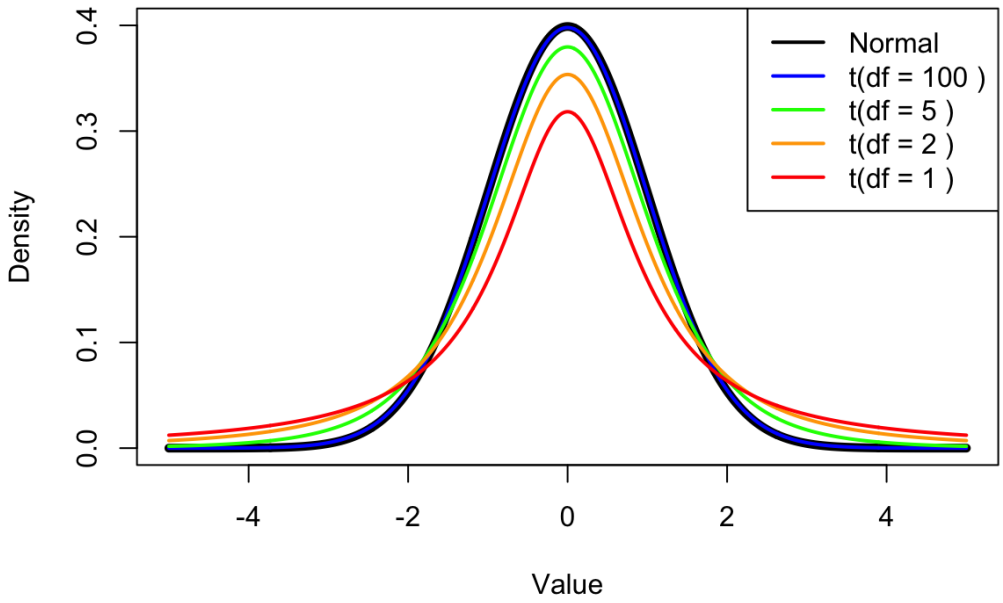

Figure 6: Density of t-distribution for v = (100, 5, 2, 1) along with standard normal distribution.

The robustness of the Kalman filter when the system noise deviates from the Gaussian assumption is investigated. Specifically, the system noise $e_{1,t}$ was simulated from a student's t-distribution with varying degrees of freedom ($\nu \in \{100, 5, 2, 1\}$). Figure 6 shows that the lower the degrees of freedom ν, the heavier the tails of the distribution, leading to a higher likelihood of extreme values.

The Kalman filter and maximum likelihood estimation were applied, however still under the assumption of Gaussian noise. The parameter estimation results for different degrees of freedom are shown in Figure 7. The results show that for $\nu = 100$, where the t-distribution closely approximates a normal distribution, the parameter estimates remain accurate and stable. However, as ν decreases, the estimates become increasingly biased and dispersed. For $\nu = 2$ and $\nu = 1$, substantial deviations and estimation failures were observed. These findings reveal that the Kalman filter is sensitive to violations of the Gaussian noise assumption and does not perform well under heavy-tailed conditions.

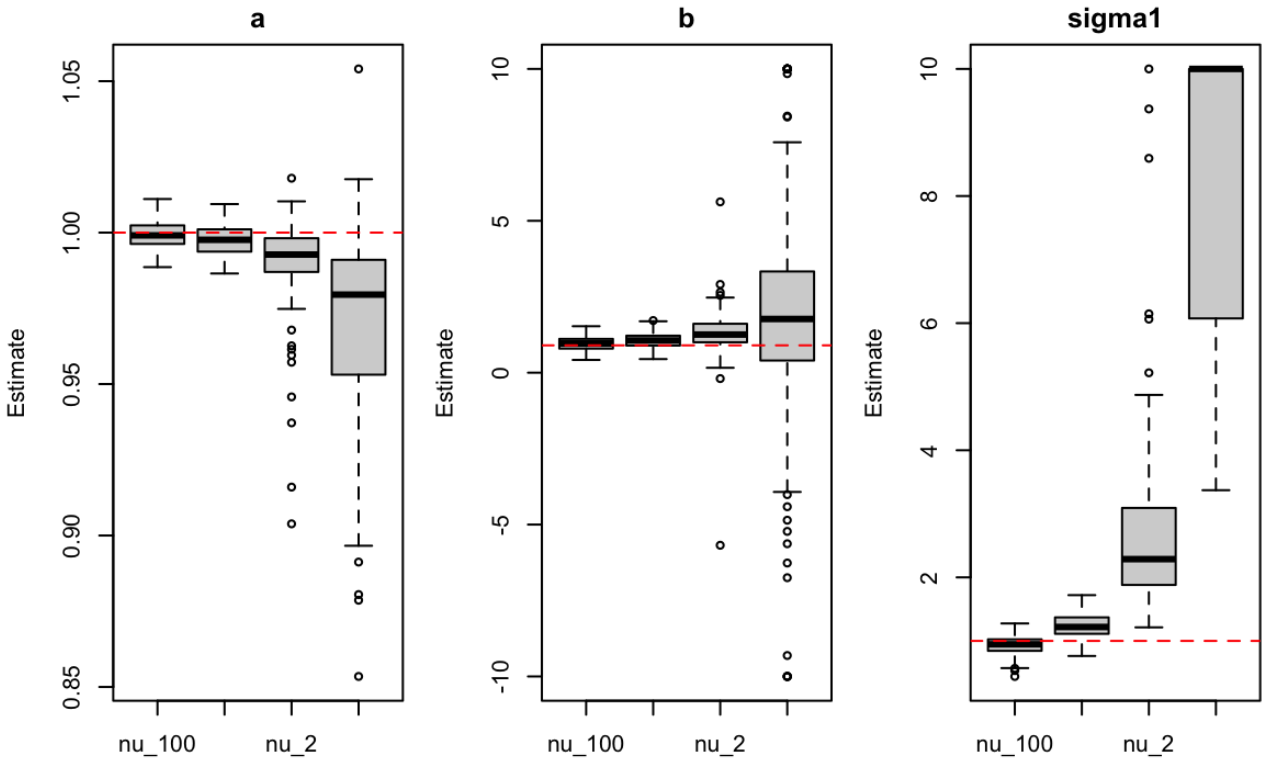

Figure 7: Parameter Estimates for Different Degrees of Freedom under Student's t-distribution

2 Parameter estimation in state-space model

2.1 Exploratory analysis of the data

Table 1 shows the Pearson correlation matrix among the 4 variables, Y_t (the temperature of the transformer station), $T_{a,t}$ (the temperature of the outdoor air), $\Phi_{s,t}$ (the horizontal global solar radiation) and $\Phi_{I,t}$ (the load on the transformer station). Correlation among the observations Y_t and other variables especially with $T_{a,t}$ and $\Phi_{s,t}$, can be noted. In addition, there is some correlation between $T_{a,t}$ and $\Phi_{s,t}$.

Table 1: Pearson's correlation among variables Y, Ta, S, and I.

	Y	Ta	S	I
Y	1.00	0.78	0.80	0.38
Ta	0.78	1.00	0.71	0.16
S	0.80	0.71	1.00	0.63
I	0.38	0.16	0.63	1.00

Figure 8 shows the temporal trend of the 4 variables Y_t, $T_{a,t}$, $\Phi_{s,t}$, $\Phi_{I,t}$. Observations are as follows;

- The transformer station temperature Y_t displays a clear diurnal trend increasing during the day and decreasing at night. Peak daytime temperature are slightly delayed compared to daytime peaks for solar radiation and load, indicating some thermal lag/inertia.
- The outdoor temperature $T_{a,t}$ also shows a strong diurnal trend. Peaks occur at or before transformer temperature peaks, suggesting it could be a driver for the system. Its temporal trend is similar to solar radiation patterns.

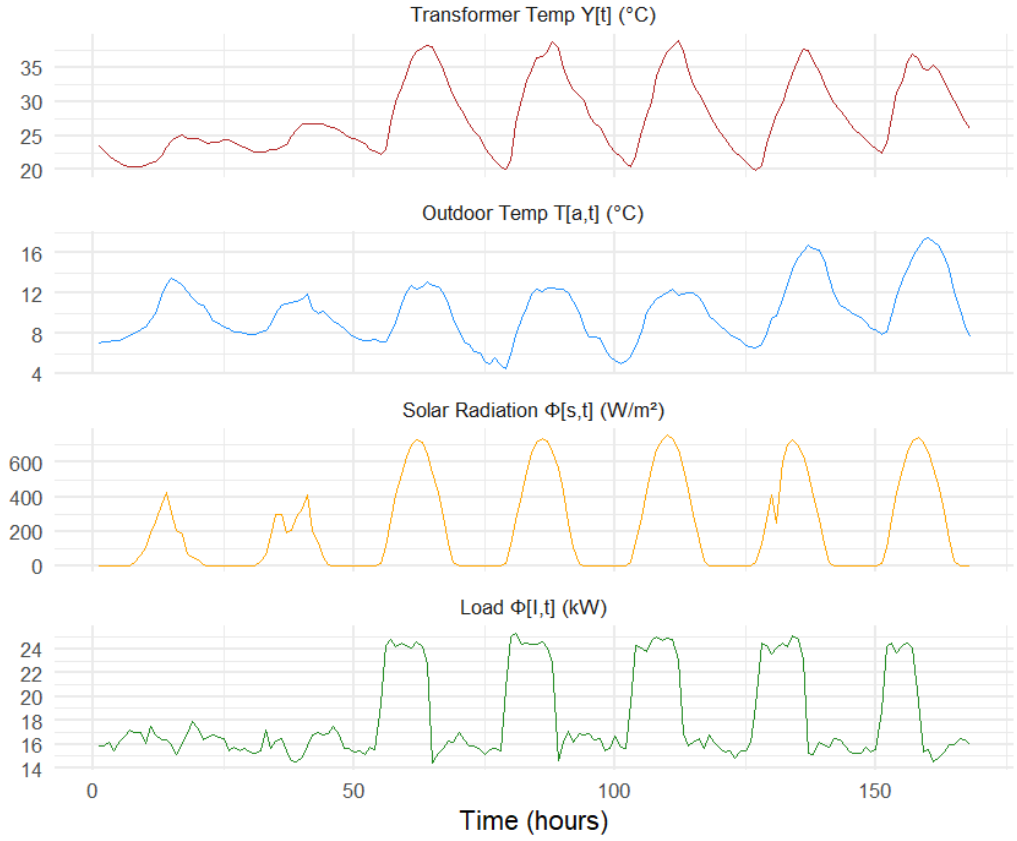

Figure 8: Time series of 4 variables: Y_t, $T_{a,t}$, $\Phi_{s,t}$, $\Phi_{I,t}$.

- Solar radiation $\Phi_{s,t}$ exhibits a regular daily pattern, peaking at midday and dropping to zero at night. The timing of its peak, prior to both outdoor and transformer temperatures, suggests it may contribute to heating indirectly by raising ambient temperatures or triggering increased load.
- The electrical load $\Phi_{I,t}$ shows a step-like pattern that likely reflects daily operational schedules, such as increased usage during work hours and reduced demand overnight. These load increases tend to align with or slightly precede peaks in transformer temperature, indicating a possible causal relationship.

2.2 Estimate a 1-D state-space model

A simple 1-D state space model was fitted to the provided data following below equations:

$$X_{t+1} = AX_t + Bu_t + e_{1,t},$$
$$Y_t = CX_t + e_{2,t},$$

where $u_t = \left[I_{a,t}, \Phi_{s,t}, \Phi_{I,t}\right]^T$ is the input vector. It is worth noting that while the estimated parameters may vary depending on the initialization and the specified lower and upper bounds, the resulting optimal values remain within a similar range and order of magnitude, indicating stability in the estimation process.

Model performance & residual analysis: Figure 9 shows the simulated one-step predictions and observed temperature along with residual analysis for the 1D state-space model. The diagnostic plots include the residual time series, QQ-plot, ACF, and PACF. **The model achieved a negative log-likelihood of -165.51, with AIC = 347.01 and BIC = 372.00.** The optimal parameter estimates are summarized in Table 2.

Table 2: Estimated parameters for the 1D state-space model.

Parameter	Description	Estimate	Unit
A	Autoregressive coefficient	0.801	–
$B_{T_{a,t}}$	Outdoor air temperature effect	0.101	°C/°C
$B_{\Phi_{s,t}}$	Solar radiation effect	0.0028	°C/(W/m^2)
$B_{\Phi_{I,t}}$	Load effect	0.211	°C/kA
C	Observation scaling factor	1.011	–
σ_1	Process noise SD	0.512	°C
σ_2	Observation noise SD	0.0083	°C

The units of the B coefficients correspond to their respective input variables. For instance, $B_{T_{a,t}} = 0.101$ °C/°C implies that a 1 °C increase in outdoor air temperature would result in an estimated 0.101 °C increase in transformer temperature. This magnitude is consistent with expectations for a system exhibiting thermal inertia.

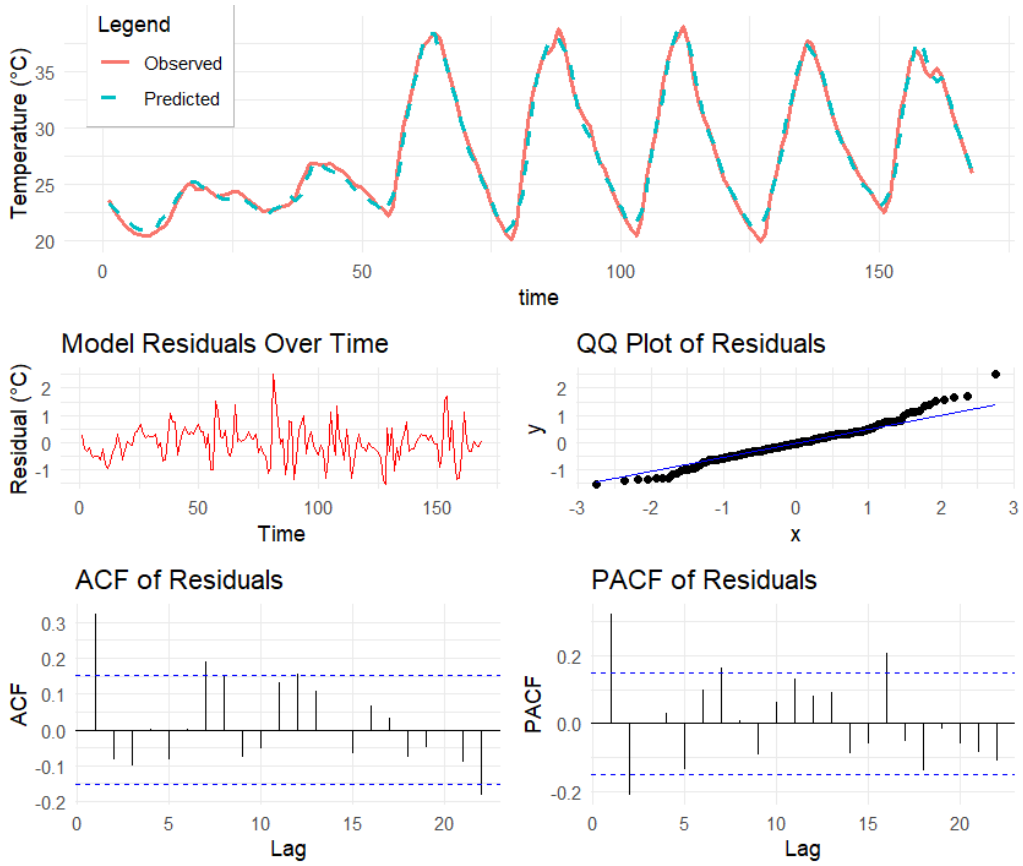

Figure 9: Observed and predicted transformer temperature: 1D state-space model.

Discussion and physical interpretation of parameters:

The 1D state-space model captures the overall dynamics of the transformer temperature well, including the diurnal patterns and daily peaks observed in the data. The residuals are approximately Gaussian but exhibit slightly heavy tails, suggesting the presence of a few outliers. These may occur at the beginning of the simulation or during instances when the model underperforms - for example, around time step 75, where it appears to underpredict a valley in the observed series.

The ACF and PACF plots indicate some residual autocorrelation at multiple lags, implying that not all temporal dependencies are fully captured by the model. This suggests potential room for improvement, possibly by introducing a more complex latent structure.

Regarding the estimated parameters, the most influential predictor is the electrical load $\Phi_{I,t}$, which is physically intuitive given that electrical load directly contributes to heat generation within

the transformer. This is followed by the outdoor air temperature $T_{a,t}$ and, lastly, solar radiation $\Phi_{s,t}$.

Although exploratory correlation analysis showed that solar radiation has the strongest Pearson correlation with transformer temperature, its regression coefficient in the state-space model is the smallest. This is likely because Pearson correlation reflects overall co-movement, whereas the regression coefficient reflects the marginal contribution of each input in the context of a one-step prediction. Since solar radiation and temperature share a strong diurnal cycle, their correlation is high. However, after accounting for the effects of electrical load and ambient temperature, which also follow the daily cycle and have more direct physical influence, the incremental predictive power of solar radiation is limited.

2.3 Expand to a 2-dimensional state-space model

The 2-D state space model was constructed based on the 1-D state space model above. Again, depending on the initialization and the lower/upper bound set for each parameters, the optimal parameters change, hence effecting the resulting re-constructed latent states, but not the overall model fit of Y_t. This indicates that without careful considerations, the Kalman filter for 2-D state space model might run into issues of finding local minimum instead of global one. The following approach was used:

- Step 1: The A, B, C and σ matrices were initialized based on the parameters obtained from 1-D state model. The lower and upper bounds were set to be the same range as in 1-D state model.
- Step 2: The model was iterated over 2000 iterations. If the optim() function could not find an optimal solutions after 2000 iterations, use the fitted parameters at the end of the 2000 iterations as the starting point and continue using the optim() function until it converges.
- Step 3: The parameters were checked if they 'hang' at upper/lower limits. If there are such parameters, revert to Step 1 by increasing the lower/upper bound and re-run the optim() function from start.

Model performance & residual analysis: Figure 10 shows the simulated and observed temperature along with residuals analysis for the 2-D state-space model which includes time series, QQ-plot, ACF and PACF of residuals. The model performance showed a **negative log-like = -123.51 with AIC = 283.03, BIC = 339.26.** The optimal parameters found are as follows:

- $A = \begin{bmatrix} 0.452 & 0.093 \\ 1.162 & 0.329 \end{bmatrix}$
- $B = \begin{bmatrix} 0.300 & 0.003 & 0.484 \\ -0.469 & -0.00097 & -0.479 \end{bmatrix}$
- $C = \begin{bmatrix} 0.577 & 0.439 \end{bmatrix}$
- $\sigma_1 = \begin{bmatrix} 0.667 & 0 \\ 0 & 0.072 \end{bmatrix}$
- $\sigma_2 = 0.0020$

Discussion & Physical interpretation: The 2-D state space model, similar to 1-D one above, performs well as it captures well the temporal dynamics of the observed data. The lower log likelihood and AIC/BIC values represents a substantial improvement in model performance, indicating that the added complexity of the 2D latent structure is justified. Residual diagnostics further support the adequacy of the model. The residual time series appears centered and shows no major structural deviations. The QQ plot indicates approximate normality, with only mild deviations in the tails. The ACF and PACF plots show small peaks, but overall a better fit than the 1D model.

From a physical standpoint, the introduction of two latent states enables the model to represent distinct thermodynamic processes within the transformer system. Comparing the parameters for the two models, State 1's parameters for the 2-D state space model is largely similar to the parameters in 1-D state space model, i.e. first row of matrix B and first column of matrix A. The main difference between the two models is the added State 2. It has negative coefficients for all variables (see second row of matrix B). The opposite signs between State 1 compared to State 2 suggests opposing physical phenomenon, e.g. State 1 as heating of the station transformer and State 2 as the cooling phase.

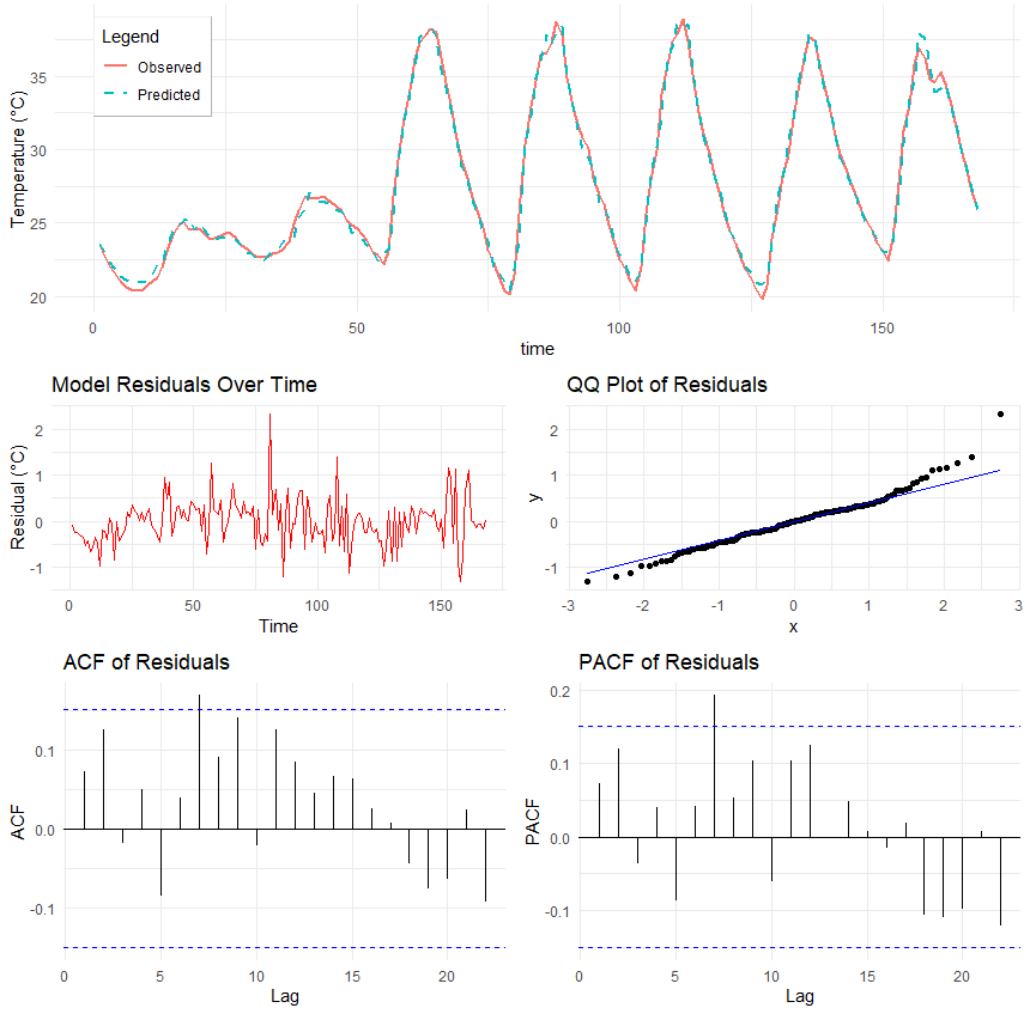

Figure 10: Observed and predicted transformer temperature: 2D state-space model.

2.4 Interpret the two reconstructed states

Figure 11 shows the reconstructed trajectories of the two latent states from the 2D state-space model, plotted alongside the scaled input variables: outdoor air temperature ($T_{a,t}$), solar radiation ($\Phi_{s,t}$), and electrical load ($\Phi_{I,t}$). The latent states display distinct temporal behaviors, suggesting that they represent different thermodynamic components of the transformer system.

- *State 1* evolves more gradually over time, with smoother transitions and broader peaks. It appears to integrate the effects of outdoor temperature and electrical load, aligning with a slowly responding component such as the transformer's core temperature. The timing of its peaks tends to lag slightly behind those of the inputs, consistent with heat accumulation and delayed thermal response.

- *State 2*, in contrast, reacts more rapidly to changes in the inputs-particularly solar radiation and electrical load, as further discussed later. It exhibits sharper peaks aligned with input fluctuations, suggesting that State 2 may represent a faster-responding surface or buffer layer, possibly linked to cooling or environmental dissipation effects.

The dynamics of the two states support a physically plausible decomposition: State 1 reflects the slower, cumulative heating of the transformer system, while State 2 captures faster-reacting thermal behavior.

Mathematically, matrix A, the state matrix, is the coefficient to predict the next latent state. Its eigenvalues λ_i, i.e. the diagonal elements determine how quickly each state changes. In this study,

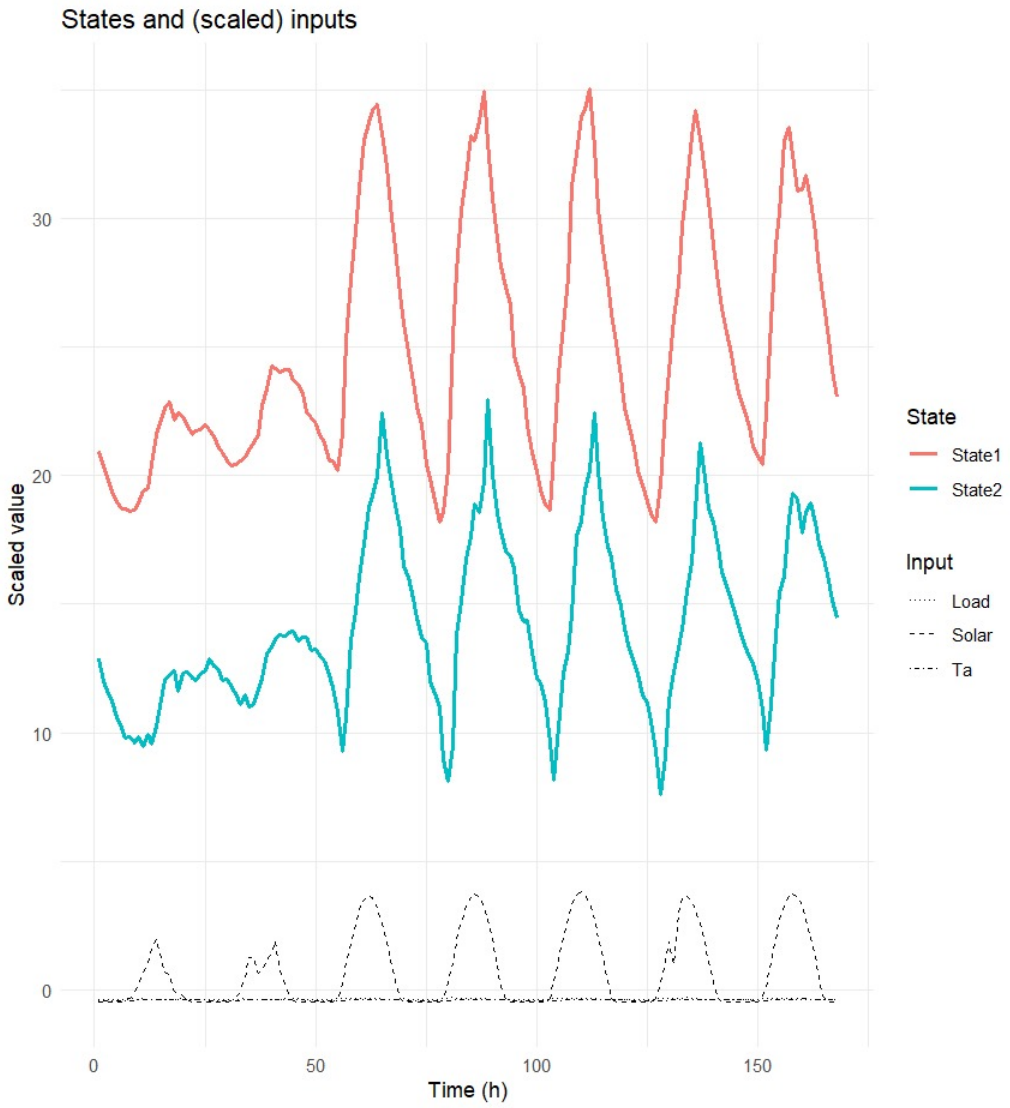

Figure 11: Two reconstructed state trajectories over time with input variables

diagonal term a_{11} and a_{22} is 0.452 and 0.329 respectively which could be interpreted as 45% of State 1 and 33% of State 2 influence the latent states in the next time step.

Matrix B indicates how each exogenous input at time t adds heat to each latent state during the next time step. Matrix B is a 2x3 matrix with 2 rows representing 2 latent states and 3 columns representing coefficients for 3 input variables ($T_{a,t}$, $\Phi_{s,t}$, $\Phi_{I,t}$). For outdoor air temperature $T_{a,t}$, higher coefficient on State 1 and smaller for State 2 suggests that air temperature affects State 1 more than State 2. For solar radiation, smaller absolute value for coefficient in State 1 and higher in State 2 suggests solar energy has a higher impact on State 2 and in a opposite manner compared to State 1. For electrical load, it has higher impact in State 1 rather than State 2. Based on this, it is suggested that State 1 is mainly driven by electrical load and outdoor air temperature but minimally by solar radiation whereas State 2 is mainly driven by the inverse of solar radiation, indicating that State 1 is likely the core transformer temperature (driven by electrical load and air temperature) and State 2 is the convective cooling (i.e. dominant at night, inverse of solar radiation peaks).

Together, the latent states allow the model to represent both long-term heating and short-term thermal responses, providing a more interpretable and realistic description of the system's behavior.